

# Multilayer roughness and image formation in the Schwarzschild objective

S. Singh, H. Solak, and F. Cerrina

University of Wisconsin, 3731 Schneider Drive, Stoughton, WI 53589

(Presented on 19 October 1995)

We present a study of the effect of multilayer surface roughness-induced scattering in the image formation of the Schwarzschild objective (SO) used in the spectromicroscope MAXIMUM. The two mirrors comprising the SO are coated with Ru/B<sub>4</sub>C multilayers that have a peak reflectivity at 130 eV. We had long observed that a diffuse x-ray background surrounds the focused x-ray spot. The spatial resolution remains at 0.1  $\mu\text{m}$  in spite of this. However, since a significant fraction of the flux is lost to the background, since too large an area of the sample is illuminated, and since the S/N ratio is degraded, the origins of this effect merit investigation. This diffuse background resulting from x-ray scattering at the surface of the mirrors was mapped out using bidirectional knife edge scans. Complementary surface roughness simulations were carried out with the ray-tracing program SHADOW. AFM experiments were also done to directly measure the surface roughness and power spectrum of representative multilayers. Following curve fitting, it was possible to classify Gaussian components in both the measured and simulated profiles as arising from scattering occurring at either the convex primary mirror or the concave secondary mirror. Together with geometrical analysis, these techniques permitted us to track the image formation process of an actual optical system in the presence of surface roughness. © 1996 American Institute of Physics.

## I. INTRODUCTION

Surface roughness and the resulting scattering and loss of flux are important issues in x-ray optics. The quality of substrate surfaces is essential not only to grazing incidence metal surface mirrors but also to normal incidence multilayer mirrors such as those comprising the Schwarzschild objective (SO) used in our x-ray photoemission spectromicroscope MAXIMUM. Multilayer coatings may be roughened at the interfaces because of substrate roughness. A variation in the layer thicknesses can introduce a phase change and affect the Bragg reflection rules. It has been shown that multilayer coating can tarnish<sup>1</sup> over time, leading to a surface roughening. This too may introduce a surface phase shift in the reflected light, resulting in yet more scattering. Regardless of its place of origin in the multilayer coating, undesired scattering from the mirrors causes a significant fraction of the x-rays incident on the SO to not be focused; instead, this scattered light forms a halo about the focused spot. This is of concern since maximum flux at the focus is needed for microscopy and also because this diffuse background results in the collection of a photoelectron signal from an area larger than the area of interest illuminated by the focused x-rays. This affects the local energy resolution of our instrument and also decreases the signal-to-noise ratio, although it does not degrade MAXIMUM's to date spatial resolution of 0.1  $\mu\text{m}$ .<sup>2,3</sup> In this paper we present our study of roughness-induced scattering in the SO, including measurements and computer simulations.

## II. EXPERIMENTAL

MAXIMUM uses a multilayer coated Schwarzschild objective to obtain a small x-ray probe. The SO set used in this experiment was coated with Ru/B<sub>4</sub>C to reflect photons of

an energy  $h\nu = 130$  eV. In our system, undulator radiation is monochromatized by a SGM (spherical grating monochromator) and focused onto a pinhole. The SO forms a 20 times demagnified image of the pinhole in its image plane. Figure 1 shows a schematic of the objective mirrors and image formation by the SO. Numerical values for the design parameters of interest of the system are listed in Table I. A spot size of 0.5  $\mu\text{m}$  was attained at the focus with the 10  $\mu\text{m}$  pinhole used.

In this study, a knife edge was scanned across the beam, like in the Foucault test used to align the microscope immediately previous to this experiment. Unlike in the Foucault test setup, however, the microscope was put out of

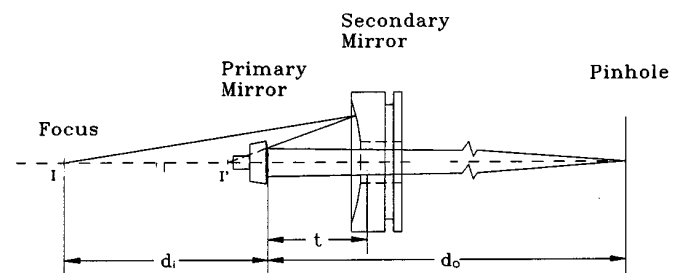


FIG. 1. SO geometry and image formation.

TABLE I. Schwarzschild objective design parameters.

Object distance ( $d_o$ )	1298 mm
Image distance ( $d_i$ )	120.78 mm
Distance between mirrors ( $t$ )	55.498 mm
Primary mirror radius of curvature	66.336 mm
Secondary mirror radius of curvature	117.253 mm

focus in order to sample more of the scattered light. In addition, MotorMikes were used instead of piezos in order to move the knife edge over a much larger range to obtain the distribution of scattered light around the focal spot. The unblocked portion of the light was viewed using a conductive phosphor screen in conjunction with a chevron MCP (microchannel plate) detector. Pulse counting electronics were used to collect the signal as a function of knife edge position. Knife edges in both the horizontal and vertical directions were used. However, due to space restrictions on the scanning stage, the scan along the horizontal direction with a vertical knife edge did not cover the entire range of the scattered radiation. The results from both knife edges looked similar. Numerical calculations, the results of which are presented here, were performed on the complete scan.

Figure 2 shows the scan in the vertical direction performed with a horizontal knife edge. The jump in the center corresponds to the specularly reflected focused light. The contribution from the specular light appears as a discontinuity on the otherwise smooth variation due to the diffuse background. Hence it is possible to accurately remove that contribution to obtain a distribution attributable only to the scattered light. This is the lower curve in Figure 2 and represents the integral of the scattered x-ray intensity over the unblocked half plane defined by the knife edge. The intensity itself in one dimension can be obtained by taking the derivative. Figure 3 shows the result of differentiation after 11 point smoothing. The contribution of the specularly reflected light can be extracted similarly by taking the difference of the derivatives of the line scans shown in Figure 2.

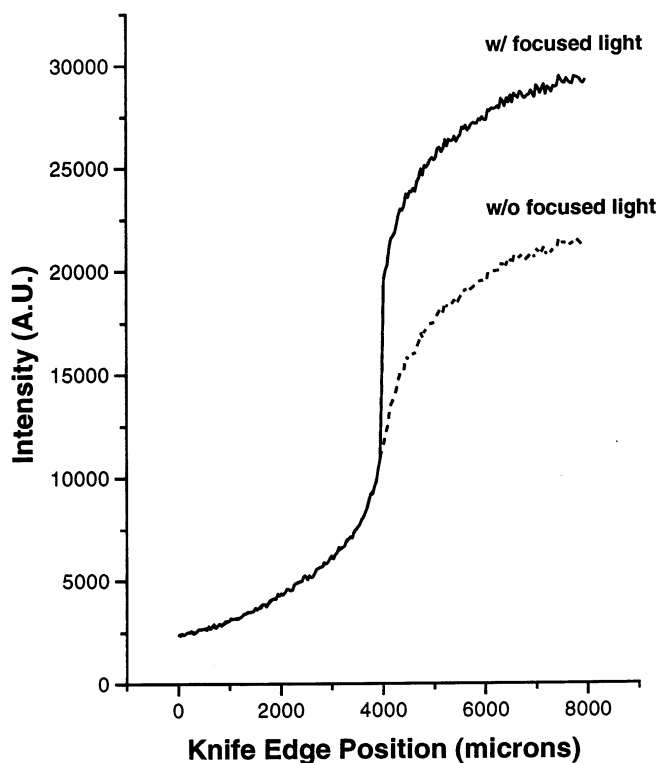


FIG. 2. Data from knife edge scan in the vertical direction, before and after removing the specular component.

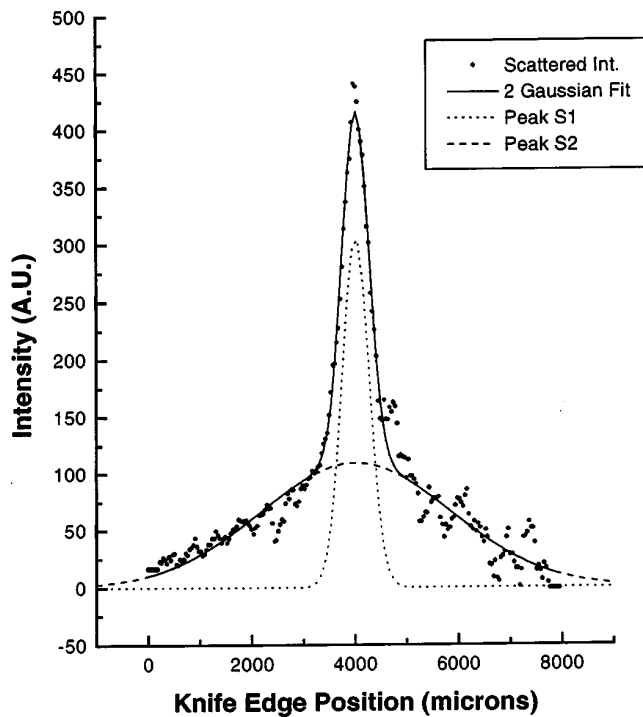


FIG. 3. Experimental scattered light intensity. Derivative of focus-removed line scan after smoothing and fitting with two Gaussian functions.

The specularly reflected light curve was integrated to obtain its contribution to the total intensity. The scattered light intensity in Figure 3 could be fitted with two Gaussian functions using a least squares algorithm. The centers were initially allowed to vary during fitting and were found to be very close, indicating that that the difference comes simply from statistical variation. Since there is also no physical reason for the centers *not* to be coincident because the scattering is an average process, the centers of the two Gaussians were forced equal during the fit. All numerical parameters are summarized in Table II. A  $\chi^2$  of 0.95 was obtained for the multiple Gaussian fit when using the level of high frequency variation in the data (in the tails) as a measure of error.

AFM (atomic force microscope) experiments were carried out on a witness sample: a Si wafer on which the multilayer pairs of Ru/B<sub>4</sub>C were RF sputter-deposited at the same time as on the SO. A TopoMetrix instrument was used. Figure 4 shows a 200 nm  $\times$  200 nm topographic image acquired in contact mode. The image has been leveled to remove piezo movement artifacts. An RMS surface roughness of 1.0 Å and

TABLE II. Numerical parameters for the specularly reflected and scattered light intensities with the microscope out of focus. A 2 Gaussian fit was done for the scattered light intensity.

Parameters	Specular	Scattered	
	Peak R	Peak S1	Peak S2
Center ( $\mu\text{m}$ )	N.A.	4015.1	4015.1
$2\sigma$ ( $\mu\text{m}$ )	N.A.	519.6	3682.0
Area (A.U.)	288350	199819	504734

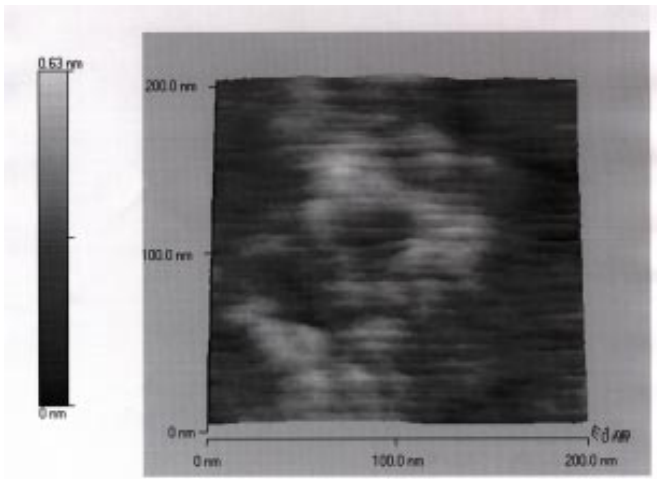


FIG. 4. 200 nm  $\times$  200 nm AFM contact mode image of witness sample of Ru/B<sub>4</sub>C.

an average height of 6.0 Å were measured. These parameters ranged from 0.9 to 2.6 Å for the RMS roughness and from 4.4 to 9.1 Å for the average height on four different areas of the sample surface. The power spectral density (PSD) computed from a 1-D surface profile of the area depicted in Figure 4 is shown in Figure 5. This PSD does indeed approximate a Gaussian function (with a  $\sigma$  of 64457 cm<sup>-1</sup>) but is plotted here on a log-log scale to bring out the high frequency features. It may be used as a representative PSD of the multilayers themselves, without the effect of any roughness present on the uncoated Schwarzschild objective mirrors themselves before the multilayer coating was deposited. AFM experiments on unoxidized Mo/Si multilayers used for the SO in the past indicated a PSD with a  $\sigma$  of 75000 cm<sup>-1</sup> and an RMS roughness of  $\sim$  10Å.

### III. PHYSICAL MODEL

The imaging properties of “rough” surfaces have been studied numerous times.<sup>4,5</sup> Many of the same techniques can be applied to optics coated with multilayers. In general, two types of roughness scattering processes may be separated out. Depending on the type of intra- and interlayer correlation, the roughness may affect both specular reflectivity and scattered light. While vertically correlated roughness does not affect the integrated reflectivity much, any type of roughness will contribute to the scattering of radiation away from the specular reflection. In the case of microscopy, scattering from the multilayers contributes a halo around the central focal spot of the microscope. Carniglia<sup>6</sup> applied scalar scattering theory<sup>7</sup> to multilayers and calculated reflected and transmitted scattering at the various interfaces in the small roughness limit. A multilayer stack model was used for various degrees of interface correlation in an approach taken by Elson et al.<sup>8</sup> A vector scattering theory<sup>7</sup> was used in conjunction with an experimental PSD function to make predictions of the

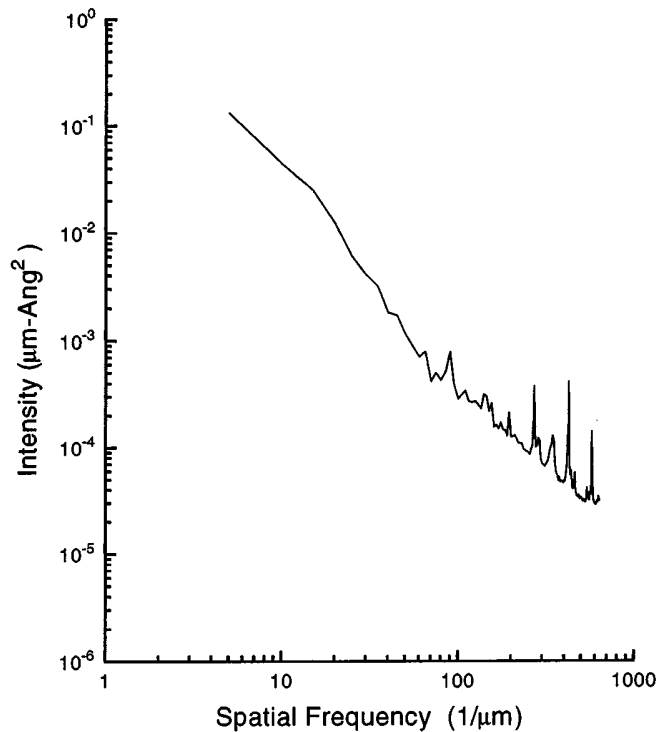


FIG. 5. Experimental power spectral density function computed from AFM surface profile.

angular distribution of scattered light. From modified Born approximation approaches<sup>9-11</sup> to a kinematical approximation treating imperfect multilayers<sup>12</sup> to efforts centered around power spectral density function,<sup>13,14</sup> much has been done. Harvey<sup>15</sup> uses a version of the PSD approach and defines a surface power spectral density filter function for the multilayer surface.

In our case, we use a standard treatment based on the power spectrum of the surface error to represent the scattering process. This use of surface transfer functions (such as the PSD) to model roughness induced scattering has been shown to be an accurate formulation of the problem well suited to numerical calculations.<sup>15</sup> Briefly, the probability of a ray’s being elastically reflected is computed according to scalar scattering theory and is given by

$$\frac{R_{scat}}{R_{tot}} = 1 - \exp \left[ - \left( \frac{4\pi\Delta \cos(\theta_i)}{\lambda} \right)^2 \right] \quad (1)$$

where  $R_{scat}$  is the intensity of the scattered light,  $R_{tot}$  is the total intensity,  $\Delta$  is the RMS roughness,  $\theta_i$  is the incidence angle, and  $\lambda$  is the wavelength.<sup>16</sup> The scattering angle is obtained by using the power spectrum of the roughness profile. Although experimental PSDs can be used, often Gaussian approximations work very well. The validity of this approach is verified *a posteriori* by the good agreement between theory and experimental observations, namely AFM results in our case.

## IV. COMPUTER MODEL

The ray-tracing program SHADOW can calculate the effect of surface roughness-induced scattering on the image formation of an optical system.<sup>17</sup> It has been used successfully to model real mirrors.<sup>18</sup> We used SHADOW to model the effects of surface roughness in the Schwarzschild objective. The power spectral density function and root-mean-square roughness are used to determine the distribution of scattered light at the image. The rough surface is modeled by a distribution of elementary small gratings with random rulings. A ray incident on the surface is scattered according to the local ruling. Since SHADOW is a stochastic ray-tracing program, a calculation is done for each ray and a new random grating is recalculated. The normalized two-dimensional PSD is used as a probability distribution function (PDF) from which a cumulative distribution function (CDF) is computed. The CDF is used along with a random number generator to select a pair of spatial frequencies in the x and y directions distributed according to the PSD chosen by the user. This pair of frequencies is used to construct the scattering vector  $\mathbf{G}$ . Thus the PSD determines the angular distribution of the scattered light.

Since the RMS roughness affects only the percentage of rays scattered, a realistic  $\Delta$  of 15 Å was chosen for both mirrors. A Gaussian PSD was defined for a chosen spatial frequency standard deviation  $\sigma_f$ . Each iteration was carried out for 5000 rays and 500 iterations were typically carried out for each run. The specularly reflected rays were blocked by a stop and only the scattered rays were analyzed. A typical run for realistic  $\Delta = 15$  Å and  $\sigma_{f_p} = \sigma_{f_s} = 10000$  cm<sup>-1</sup> is shown in Figure 6.  $\sigma_{f_p}$  and  $\sigma_{f_s}$  are the spatial frequency  $\sigma_f$ 's for the primary and secondary mirrors, respectively. The intensity is integrated in y to yield a 1-D distribution that can be fit with two Gaussian functions for roughness on both mirrors. It was found that when the roughness is turned off on one of the mirrors, the intensity can be fit with just one Gaussian, as expected. This suggests that the scattered light distribution of a SO with two rough mirrors is a convolution of two Gaussians. The results of curve fitting carried out on representative SHADOW simulations are shown in Table III. The last entry in Table III is particularly interesting in that the  $\sigma_f$ 's for the primary and secondary mirror are different. We note that the ratio of the widths of the two peaks for this case is 5.42; where it is 2.7-2.8 for all other SHADOW simulations done for which the PSD  $\sigma_f$ 's were the same for both mirrors. This is true also for many simulations not included here. Figure 7 shows the scattered light distribution for the case where  $\Delta = 15$  Å,  $\sigma_{f_p} = 10000$  cm<sup>-1</sup> and  $\sigma_{f_s} = 20000$  cm<sup>-1</sup>.

## V. DISCUSSION

A ray incident on the SO can undergo different processes both on the primary and on the secondary mirrors. First, it may be absorbed. If it is not absorbed, it may be either

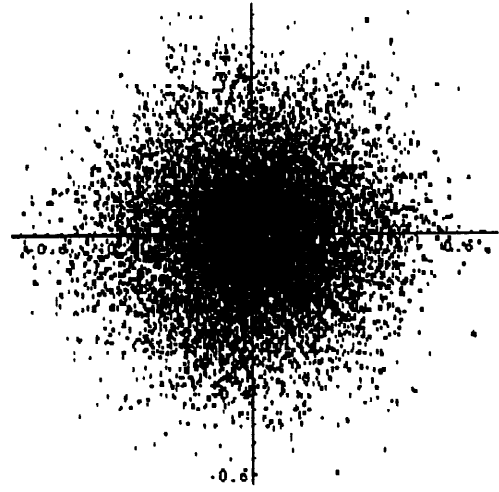


FIG. 6. Simulated spatial distribution of scattered rays at the image plane for realistic  $\Delta = 15$  Å and  $\sigma_{f_p} = \sigma_{f_s} = 10000$  cm<sup>-1</sup>.

TABLE III. Gaussian fitting parameters for the scattered light intensity computed by SHADOW for  $\Delta = 15$  Å.

$\sigma_{f_p}$ (cm <sup>-1</sup> )	$\sigma_{f_s}$ (cm <sup>-1</sup> )	$\sigma_{S1}$ (μm)	$\sigma_{S2}$ (μm)	$I_{S1}$ (A.U.)	$I_{S2}$ (A.U.)	$\sigma_{S2} / \sigma_{S1}$
10000	10000	621.9	1722.3	56552	31063	2.77
40000	40000	2485.6	6921.0	48833	26373	2.78
75000	75000	4641.0	13092.5	46917	24518	2.82
10000	20000	623.7	3378.9	79376	22846	5.42

$\sigma_{f_p} = 10000$  cm<sup>-1</sup> and  $\sigma_{f_s} = 20000$  cm<sup>-1</sup>. This distribution looks very similar to the experimental data shown in Figure 3.

specularly reflected or scattered. This may occur at either mirror. We identify as **R** those rays specularly reflected by both mirrors. Those reflected at the primary mirror but scattered at the secondary are labeled as **S** while those scattered at the primary mirror but reflected at the secondary are called **P**. Rays scattered by both mirrors are labeled **D**, for doubly scattered. The diagram in Figure 8 shows these processes.  $r_p$  ( $r_s$ ) is the reflectivity of the primary (secondary) mirror.  $k_p$  ( $k_s$ ) is the probability that a ray that is not absorbed will be scattered. Following the scheme in Figure 8, the relative strengths of the four components may be written as

$$R : P : S : D = (1 - k_p)(1 - k_s) : k_p(1 - k_s) : (1 - k_p)k_s : k_p k_s \quad (2)$$

The reflectivities  $r_p$  and  $r_s$  do not appear in the above equation and hence have no effect on the distribution of light. This fact allowed us to discard the effects of losses in the SHADOW simulations. It is interesting to note that, assuming that both mirrors have equal scattering coefficients, scattered light in the image plane will have equal

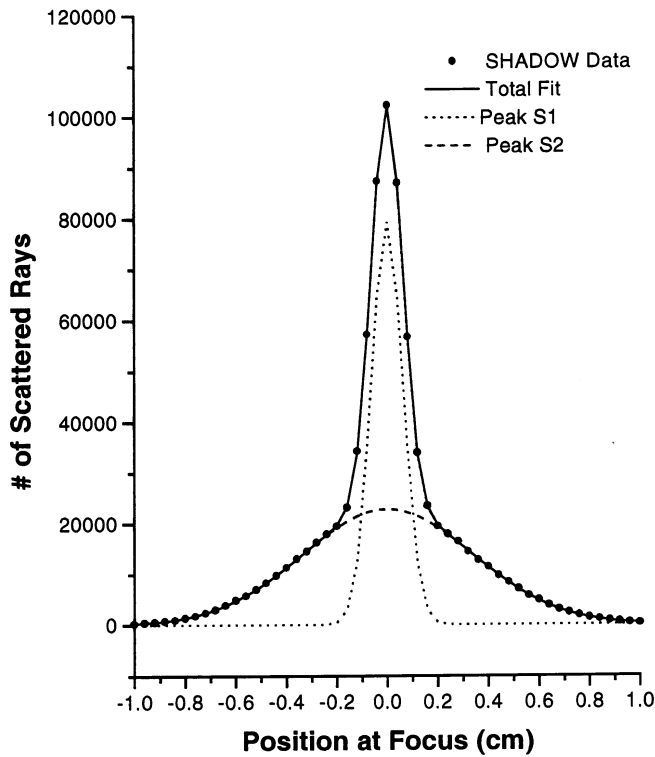


FIG. 7. Simulated scattered light intensity for  $\Delta = 15 \text{ \AA}$ ,  $\sigma_{fp} = 10000 \text{ cm}^{-1}$  and  $\sigma_{fs} = 20000 \text{ cm}^{-1}$ .

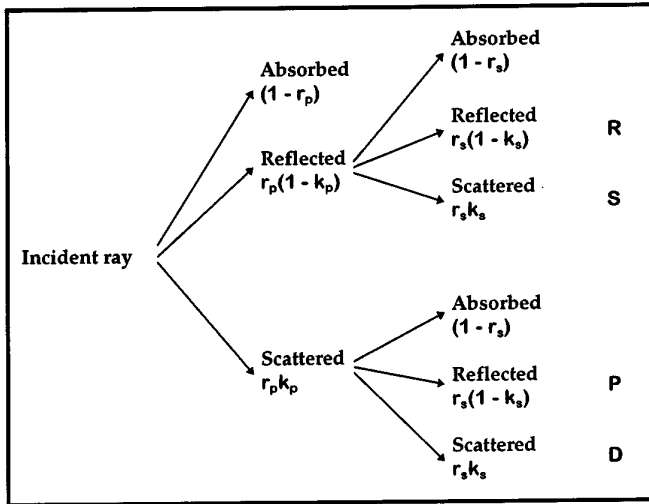


FIG. 8. Tree showing different paths that a ray can take in the SO system.

contributions from the two mirrors. We can also deduce from the above equation that for an  $N$  mirror system the relative strength of specularly reflected light will be  $(1 - k)^N$  assuming a uniform scattering coefficient  $k$  for all mirrors. This implies that losses due to scattering may quickly become limiting in a multimirror imaging system.

As seen earlier, the distribution of scattered light measured could be fit with two diffuse Gaussians. We will show in this article that the doubly scattered light has the shape and intensity of the convolution of the two singly scattered

components. The ratio of widths of the two Gaussian components  $S2$  and  $S1$  identified in the experimental data was  $\sigma_{S2}/\sigma_{S1} = 7.1$ . Since the  $\sigma$  of the convolution of the two Gaussians would be within  $\sim 1\%$  of  $\sigma_{S2}$ , it was not possible to resolve it separately. We conclude therefore that the wider Gaussian  $S2$  shown in Figure 3 is a combination of two scattered light distributions: that of light scattered only by the secondary mirror (**S**) and that of doubly scattered (**D**) light. The narrower Gaussian  $S1$ , then, is the distribution of light scattered only by the primary mirror (**P**).

Now Equation 2 and the experimental results may be used to estimate the scattering coefficients  $k_p$  and  $k_s$  for the SO. Note that equation 2 is actually three equations in the two unknowns  $k_p$  and  $k_s$ . From the ratios of the areas of the Gaussian fits to the experimental data, we have

$$\frac{P}{D + S} = 0.396 \quad (3)$$

$$\frac{R}{D + P + S} = 0.409 \quad (4)$$

Solving equations 2, 3, and 4 together, we obtain

$$k_p = 0.41, \quad k_s = 0.50 \quad (5)$$

It appears that more light is scattered by the secondary mirror than by the primary. It should be noted that the two components **S** and **D** were not resolved in SHADOW results either.

The effect of scattering on the SO system can be easily treated with matrix optics by the introduction of random angles to account for the scattering process. Usage of matrix optics is justified for the SO because of the small angles between the rays and the optical axis and the circular symmetry of the SO. Using the notation in Figure 1 for distances, we introduce the following five matrices:  $T_1$  for transmission from the pinhole to the primary,  $R_1$  for reflection from the primary,  $T_2$  for transmission from the primary to the secondary,  $R_2$  reflection from the secondary, and, finally,  $T_3$  for transmission from the secondary to the image plane.

$$T_1 = \begin{bmatrix} 1 & d_o \\ 0 & 1 \end{bmatrix}, R_1 = \begin{bmatrix} 1 & 0 \\ \frac{2}{R_p} & 1 \end{bmatrix}, T_2 = \begin{bmatrix} 1 & t \\ 0 & 1 \end{bmatrix} \quad (6)$$

$$R_2 = \begin{bmatrix} 1 & 0 \\ -\frac{2}{R_s} & 1 \end{bmatrix}, T_3 = \begin{bmatrix} 1 & d_i + t \\ 0 & 1 \end{bmatrix}.$$

A ray with initial coordinates  $y_0, \theta_0$  on the pinhole plane is transferred to the image plane according to the equation

$$\begin{bmatrix} y_i \\ \theta_i \end{bmatrix} = T_3 R_2 T_2 R_1 T_1 \begin{bmatrix} y_o \\ \theta_o \end{bmatrix} = \mathbf{M} \begin{bmatrix} y_o \\ \theta_o \end{bmatrix} = \begin{bmatrix} m_{11} & m_{12} \\ m_{21} & m_{22} \end{bmatrix} \begin{bmatrix} y_o \\ \theta_o \end{bmatrix} \quad (7)$$

if we disregard the effect of scattering. Then we have  $m_{12} = -6.46594 \times 10^{-16} \approx 0$ ,  $m_{11} = -0.05$ , and  $m_{22} = -20.00$  as expected at a conjugate plane for a system with a demagnification of 20. We also have  $m_{21} = -0.015$ , the power of the system.  $m_{21}$  must, in fact, be nonzero for an imaging system.<sup>19</sup> We can include scattering in this equation by adding random angles  $\tilde{\delta}_s$  and  $\tilde{\delta}_p$  to the angle coordinates of rays after reflections from the primary and secondary mirrors.

$$\begin{bmatrix} y_i \\ \theta_i \end{bmatrix} = T_3 \left( \begin{bmatrix} 0 \\ \tilde{\delta}_s \end{bmatrix} + R_2 T_2 \left( \begin{bmatrix} 0 \\ \tilde{\delta}_p \end{bmatrix} + R_1 T_1 \begin{bmatrix} y_o \\ \theta_o \end{bmatrix} \right) \right). \quad (8)$$

This yields

$$\begin{bmatrix} y_i \\ \theta_i \end{bmatrix} = \mathbf{M} \begin{bmatrix} y_o \\ \theta_o \end{bmatrix} + \begin{bmatrix} a & b \\ c & d \end{bmatrix} \begin{bmatrix} \tilde{\delta}_p \\ \tilde{\delta}_s \end{bmatrix}, \quad (9)$$

where  $a = 64.9049$ ,  $b = 176.281$ ,  $c = 0.05336$ , and  $d = 1$ . For a point source ( $y_o = 0$ ) we may write

$$y_i = a\tilde{\delta}_{p+b} + b\tilde{\delta}_s. \quad (10)$$

Probability density functions (PDFs) of  $\tilde{\delta}_s$  and  $\tilde{\delta}_p$  depend in general on the angle of incidence  $\theta_o$ . For near normal incidence, we can assume that PDFs for  $\tilde{\delta}_s$  and  $\tilde{\delta}_p$  have no dependence on  $\theta_o$ . If both mirrors had no scattering, the additive random angles  $\tilde{\delta}_s$  and  $\tilde{\delta}_p$  would have PDFs that were Dirac delta functions, i.e., both  $\tilde{\delta}_s$  and  $\tilde{\delta}_p$  would be equal to zero. Then we retrieve equation 7. Estimating the PDF of scattering angle  $\theta$  as having a Gaussian distribution, an assumption borne out by the AFM PSDs, for the primary (secondary) mirror we can write the PDF for  $\tilde{\delta}_p$  as,

$$f_{\tilde{\delta}_{p(s)}}(\theta) = (1 - k_{p(s)})\delta(\theta) + \frac{k_{p(s)}}{\sqrt{2\pi\sigma_{p(s)}}} \exp\left[-\frac{\theta^2}{2\sigma_{p(s)}^2}\right], \quad (11)$$

where  $k_{p(s)}$  is the scattering coefficient as defined earlier,  $\sigma_{p(s)}$  is the standard deviation of the scattering angle, and  $\delta(\theta)$  is the Dirac delta function. We may rewrite these PSDs in terms of the position  $y$  at the focus by simply multiplying  $\sigma_p$  and  $\sigma_s$  by the factors of  $\tilde{\delta}_s$  and  $\tilde{\delta}_p$  in equation 10. Upon taking their convolution, we obtain the following PDF for the light distribution in the focal plane.

$$\begin{aligned} f(y) = & (1 - k_p)(1 - k_s)\delta(y) \\ & + \frac{k_p(1 - k_s)}{\sqrt{2\pi(a\sigma_p)}} \exp\left[\frac{-y^2}{2(a\sigma_p)^2}\right] \\ & + \frac{k_s(1 - k_p)}{\sqrt{2\pi(b\sigma_s)}} \exp\left[\frac{-y^2}{2(b\sigma_s)^2}\right] \\ & + \frac{k_p k_s}{\sqrt{2\pi\sqrt{(b\sigma_s)^2 + (a\sigma_p)^2}}} \exp\left[\frac{-y^2}{2\left((b\sigma_s)^2 + (a\sigma_p)^2\right)}\right] \end{aligned} \quad (12)$$

The terms in equation 12 correspond to the **R**, **P**, **S**, **D** terms, respectively. This result proves that the doubly scattered rays have a distribution that is equal to the convolution of the distributions of the singly scattered rays.

The ratio of widths of the two components **P** and **S** is calculated as

$$r_w = \frac{\sigma_{S2}}{\sigma_{S1}} = \frac{b\sigma_s}{a\sigma_p} \quad (13)$$

Then  $r_w = b/a = 2.72 \Leftrightarrow \sigma_s = \sigma_p$ . That this is reproduced by ray tracing simulations can be seen in the values for  $\sigma_{S2}/\sigma_{S1}$  in Table III for the case of the same PSD on both mirrors. In the grating model of scattering, the sine of the scattering angle is proportional to the local spatial frequency. If the spatial frequency is distributed according to a Gaussian PSD, then  $\sin(\theta)$  also has a Gaussian distribution with a standard deviation proportional to the standard deviation of the PSD. Since  $\sin(\theta) \sim \theta$  for small angles, we may say the same for  $\theta$  itself. Therefore, the ratio of scattering angles on the primary and secondary mirrors is equal to the ratio of the PSD  $\sigma_f$ 's corresponding to the two mirrors. We may write

$$r_{\sigma_{fs}/\sigma_{fp}} = \frac{\sigma_{fs}}{\sigma_{fp}} = r_w \frac{a}{b} \quad (14)$$

We know that the value of  $r_w$  is 7.1 for the experimental data. After substituting in the numerical values of  $a$  and  $b$ , we have  $r_{\sigma_{fs}/\sigma_{fp}} = 2.61$ . To accurately simulate the experimental data in SHADOW, we must choose two different PSDs for the primary and secondary mirrors in accordance with this relation. The SHADOW output in Figure 7 was an initial attempt to do this before the exact

value of  $r_{\sigma_{f_s}/\sigma_{f_p}}$  above was known. Its  $r_{\sigma_{f_s}/\sigma_{f_p}}$  was 2.0. As mentioned in the previous section, it describes well the shape of experimental scattered light distribution, but a better agreement could be obtained by using a ratio such as equation 14. A RMS roughness  $\Delta$  was calculated from equation 1 to be  $9.4 \text{ \AA}$ , a result close to the AFM measurements and that could also be utilized in a new simulation. A  $\sigma_{f_s}$  of  $10715 \text{ cm}^{-1}$  was computed from the scattering angle inferred from  $\sigma_{S2}$  and was used in a new run of SHADOW along with the exact ratio. The outcome of this final simulation is shown along with the experimental data in Figure 9. As can be seen, theoretical calculations are in excellent agreement with scattering measurements

The origin of two different PSDs on two mirrors coated with Ru/B<sub>4</sub>C at the same time may be the manufacturing process used to create the mirror blanks. Different turning and grinding techniques are used for the convex primary and concave secondary mirrors and leave different types of microroughness on the surfaces. These processes likely contribute more to correlated and uncorrelated roughness in the multilayers than the inherent roughness in the multilayers themselves. The inherent multilayer roughness would be the same for both blanks. Thus two different PSDs for the two mirrors are experimentally possible.

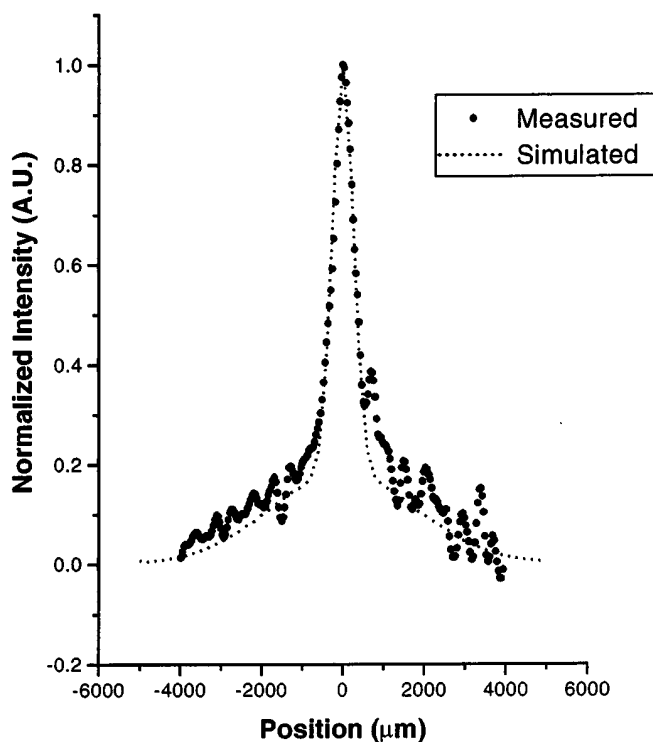


FIG. 9. Measured and simulated scattered light intensities. Simulation uses experimental roughness parameters.

## VI. CONCLUSIONS

We have seen that the experimentally measured scattered light distribution at the focus of the multilayer-coated Schwarzschild objective is composed of two components arising from scattering processes at the two mirrors. This distribution can be accurately modeled using scalar scattering theory with ray tracing in the program SHADOW. This leads to a better understanding of the image formation of a real physical system, which can be useful for, among other things, choosing surface roughness characteristics for optics designed for imaging applications. In this way we do not simply model scattering from a rough planar system and apply it to a real multimirror imaging system. Rather, we study the image formation in conjunction with scattering in a concrete optical system in order to understand the effect of scattering at the optical surfaces on the image. By this method we can obtain surface roughness parameters that can be confirmed through independent means such as AFM. All in all, we have been able to successfully model the image formation of our experimental system, the Schwarzschild objective, in the presence of surface roughness.

- 1 J.H. Underwood, E.M. Gillikson, and K. Nguyen, Tarnishing of Mo/Si Multilayer X-ray Mirrors, *Applied Optics*, **32**:6985, 1993.
- 2 W. Ng, A. K. Ray-Chaudhuri, S. Liang, S. Singh, H. Solak, J. Welak, F. Cerrina, G. Margartitondo, J.H. Underwood, J.B. Kortright, and R.C.C. Perera, High resolution spectro-microscopy reaches the 1000 Å scale, *Nucl. Instr. and Meth.*, **A347**:422, 1994.
- 3 F. Cerrina, The Role of S/N in Determining the Resolution of a Scanning X-ray Microscope, In *Proc. 6th Int'l Conf. on Electron Spectroscopy*, Journal of Electron Spectroscopy and Related Phenomena, 1995.
- 4 J.M. Bennett, editor, *Surface Finish and Its Measurement*, volume B, Optical Society of America, 1992. Many good papers.
- 5 H. Hogrefe and C. Kunz, Soft X-ray Scattering from Rough Surfaces: Experimental and Theoretical Analysis, *Applied Optics*, **26**:2851, 1987.
- 6 C.K. Carniglia, Scalar Scattering Theory for Multilayer Optical Coatings, in J.M. Bennett, editor, *Surface Finish and Its Measurement*, volume B, chapter 14, page 636, Optical Society of America, 1992.
- 7 J.A. Ogilvy, *Theory of Wave Scattering from Random Rough Surfaces*, Adam Hilger, New York, 1991.
- 8 J.M. Elson, J.P. Rahn, and J.M. Bennett, Light Scattering from Multilayer Optics: Comparison of Theory and Experiment, in J.M. Bennett, editor, *Surface Finish and its Measurement*, volume b, chapter 17, page 769, Optical Society of America, 1992.
- 9 D.G. Stearns, The Scattering of X-rays from Nonideal Multilayer Structures, *J. Appl. Phys.*, **65**:491, 1988.
- 10 Kopecký, Diffuse Scattering of X-rays from Nonideal Layered structures, *J. Appl. Phys.*, **77**:2380, 1995.

- 11 D.G. Stearns, X-ray Scattering from Interfacial Roughness in Multilayer Structures, *J. Appl. Phys.*, **71**:4286, 1992.
- 12 A. Bruson, X-ray Scattering from Nonideal Multilayer Structures: Calculations in the Kinematical Approximation, *Appl. Phys.*, **77**:1001, 1995.
- 13 E. Spiller, D. Stearns, and M. Krumrey, Multilayer X-ray Mirrors: Interfacial Roughness, Scattering, and Image Quality, *J. Appl. Phys.*, **74**:107, 1993.
- 14 J.M. Elson and J.M. Bennett, Calculation of the Power Spectral Density from Surface Profile Data, *Applied Optics*, **34**:201, 1995.
- 15 J.E. Harvey, Modeling the Image Quality of Enhanced Reflectance X-ray Multilayers as a Surface Power Spectral Density Filter Function, *Applied Optics*, **34**:3715, 1995.
- 16 J.M. Bennett and L. Mattsson, *Introduction to Surface Roughness and Scattering*, Optical Society of America, 1989.
- 17 C. Welnak, P. Anderson, M. Khan, S. Singh, and F. Cerrina, Recent Development in SHADOW, *Rev. Sci. Instrum.*, **63**:865, 1992.
- 18 G.M. Wells, R. Nachman, C. Welnak, S. Singh, J. Guo, M. Khan, S. Turner, F. Cerrina, Y. Vladimirovsky, and J. Maldonado, Effects of Mirror Surface Roughness on Exposure Field Uniformity in Synchrotron X-ray Lithography, *J. Vac. Sci. Technol. B*, **9**:3227, 1991.
- 19 M.V. Klein and T.E. Furtak, *Optics*, chapter 3, "Geometrical Optics", page 160, John Wiley and Sons, New York, 2nd edition, 1986.